BUTTERWORTH HEINEMANN

Polymer Vol. 36 No. 7, pp. 1455–1467, 1995

0032-3861/95/$10.00 + 0.00

Correlations for the quiescent crystallization kinetics of isotactic polypropylene and poly(ethylene terephthalate)

C. A. Hieber
Sibley School of Mechanical & Aerospace Engineering, Cornell University, Ithaca, NY 14853, USA
(Received 5 July 1994)

The Nakamura equation is used to generate a direct relation (first-order differential equation) between the Avrami and Ozawa crystallization rate constants. As a result, it is possible to compare isothermal and constant-cooling-rate crystallization data in a consistent manner. This is done for isotactic polypropylene (i-PP) and poly(ethylene terephthalate), based upon data available from the literature. Resulting correlations are obtained for these two materials at atmospheric pressure as well as for i-PP at elevated pressure. The results corroborate that the maximum crystallization rate occurs approximately midway between the glass-transition and melting temperatures. In addition, the results imply that there is no need to explicitly incorporate an induction time when the modelling is based upon the Nakamura equation.

(Keywords: crystallization kinetics; isotactic polypropylene; poly(ethylene terephthalate))

INTRODUCTION

In analysing the crystallization kinetics of polymers, one underlying consideration is to establish whether data obtained under isothermal conditions are indeed compatible with measurements obtained under constant-cooling-rate conditions. In the present paper, we make use of the well-known Nakamura[1,2] model as a basis for establishing the link between the Avrami[3,4] limit under isothermal conditions and the Ozawa[5] limit under constant-cooling-rate conditions. By manipulating such models, a basis is presented for directly relating isothermal and constant-cooling-rate crystallization data. It is noted that this correlation between the two types of data is established without any need for explicitly incorporating an induction time. The approach is illustrated by detailed application to available data for isotactic polypropylene (i-PP) and for poly(ethylene terephthalate) (PET), including the effect of elevated pressure for i-PP.

MODELLING CONSIDERATIONS

For the case of isothermal crystallization, the classical modelling is that usually attributed to Avrami[3,4], where the relative crystallinity is given by

$$\chi = 1 - \exp[-k(T)t^n] \tag{1}$$

where $k(T)$ is the Avrami rate constant and n is the Avrami index, typically lying between 2 and 4. In an analogous manner, for constant-cooling-rate crystallization, the classical modelling of Ozawa[5] is given by

$$\chi = 1 - \exp\left[-\frac{\kappa(T)}{\varphi^n}\right] \tag{2}$$

where $\kappa(T)$ is the Ozawa rate constant and $\varphi \equiv -\partial T/\partial t$ is the constant cooling rate. Of course, if one is to include the effect of elevated pressure, then presumably k and κ will be functions of both T and p, as will be treated later in the Appendix. For the time being, however, it will be convenient to omit the pressure dependence.

As a generalization of the Avrami equation (1) to non-isothermal situations, the equation of Nakamura *et al.*[1,2] is given by

$$\chi = 1 - \exp\left\{-\left[\int_0^t K(T)\,\mathrm{d}t\right]^n\right\} \tag{3}$$

In the isothermal case, this is seen to reduce to equation (1) with

$$K^n(T) = \mathrm{k}(T) \tag{4}$$

On the other hand, in the constant-cooling-rate case, one has that

$$\mathrm{d}t = -\frac{\mathrm{d}T}{\varphi} \tag{5}$$

where φ is a constant such that equation (3) reduces to equation (2) with

$$\left[\int_T^{T_i} K(\tilde{T})\,\mathrm{d}\tilde{T}\right]^n = \kappa(T) \tag{6}$$

where T_i denotes the initial temperature taken sufficiently high above the melting temperature, T_m, where the rate constant is vanishingly small.

Accordingly, it is seen that the Nakamura equation (3) contains both the Avrami (equation (1)) and Ozawa (equation (2)) limits. Importantly, the Nakamura equation

can therefore be used as a basis for relating the Avrami and Ozawa model parameters. In particular, from equations (4) and (6) it follows that

$$\left[\int_T^{T_i} k^{1/n}(\tilde{T})\,d\tilde{T}\right]^n = \kappa(T) \tag{7}$$

Accordingly, it is convenient to introduce

$$\sigma(T) \equiv \kappa^{1/n}(T) \tag{8}$$

such that

$$\int_T^{T_i} k^{1/n}(\tilde{T})\,d\tilde{T} = \sigma(T) \tag{9}$$

Further, if one differentiates equation (9) with respect to T and introduces

$$\lambda(T) \equiv k^{-1/n}(T) \tag{10}$$

it then follows that

$$\frac{d\sigma}{dT} = -\frac{1}{\lambda(T)} \tag{11}$$

Accordingly, if one starts at sufficiently large T above T_m, where $k(T)$ and $\kappa(T)$ are vanishingly small (such that σ and λ^{-1} are also vanishingly small), one can then use equation (11) to determine $\sigma(T)$, if $\lambda(T)$ is known, by simply marching forward in (decreasing) temperature. Alternatively, if $\sigma(T)$ is known, we can then determine $\lambda(T)$ directly, namely

$$\lambda(T) = -\frac{1}{d\sigma/dT} \tag{12}$$

Curiously, although these relations have been obtained by simple manipulations, the present author is unaware of any previous investigation in which such relations have been used to compare isothermal and constant-cooling-rate crystallization data. This will be done in the following sections, as applied to i-PP and PET.

APPLICATION TO i-PP

Concerning the isothermal crystallization of i-PP, *Table 1* lists available experimental sources from the literature[6–32] based upon various methods, as indicated. With one exception[27], these experimental results are all at atmospheric pressure. Shown plotted in *Figure 1* are data points from these various sources in terms of $\lambda(T)$, where use

Table 1 Summary of isothermal crystallization data for isotactic polypropylene

Reference	Ref. no.	Method[a]	T(°C)	n
Falkai and Stuart (1959)	6	dilatometry	122–145	3.0
Marker *et al.* (1959)	7	dilatometry	123–156	~3.0
Griffith and Ranby (1959)	8	dilatometry	133–155	~3.0
Magill (1962)	9	LDM	62–141	~2.0 (≲115°C)
				~3.0 (>115°C)
Ishizuka (1962)	10	dilatometry	118–140	~3.0
Parrini and Corrieri (1963)	12	dilatometry	130–160	2.8–4.0
Chiu (1964)	13	d.s.c.	115–123	–
Gordon and Hillier (1965)	14	dilatometry	134–149	2.4–2.6
Hoshino *et al.* (1965)	15	dilatometry	134–143	3.0–3.5
Godovsky and Slonimsky (1966, 1974)	16, 19	d.s.c.	117–140	2.0
		dilatometry	130–137	2.9–3.1
Heyns and Heyez (1971)	17	d.s.c.	110–130	2.7–3.5
Iwanami *et al.* (1972)	18	dilatometry	128–144	2.8
		LDM	108–133	3.0
Pratt and Hobbs (1976)	20	d.s.c.	110–133	2.7–3.1
		LDM	115–127	2.9–3.0
Wlochowicz and Eder (1981)	21	i.r.s.	95–135	2.9–3.1
Rybnikar (1982)	22	LDM	137–150	~3.0
Avella *et al.* (1983)	23	d.s.c.	123–134	2.0–2.6
Martuscelli *et al.* (1984)	24	d.s.c.	122–132	1.8–2.0
Hammami (1990)	25	d.s.c.	117–126	2.0–2.6
		LDM	126–139	2.7–3.9
Ryu *et al.* (1991)	26	d.s.c.	120–130	~2.2
He and Zoller (1991)	27	pressurized dilatometry	134–191	1.3–1.7
He (1991)	28	d.s.c.	120	2.1
Tai *et al.* (1991)	29	d.s.c.	114–132	~3.0
Piccarolo *et al.* (1992)	30	d.s.c.	128–136	–
Paiz *et al.* (1993)	31	d.s.c.	130–140	5.9–7.6
Kim *et al.* (1993)	32	d.s.c.	124–136	2.4–2.7

[a] LDM, light depolarizing microscopy, i.r.s., infra-red spectroscopy, d.s.c., differential scanning calorimetry

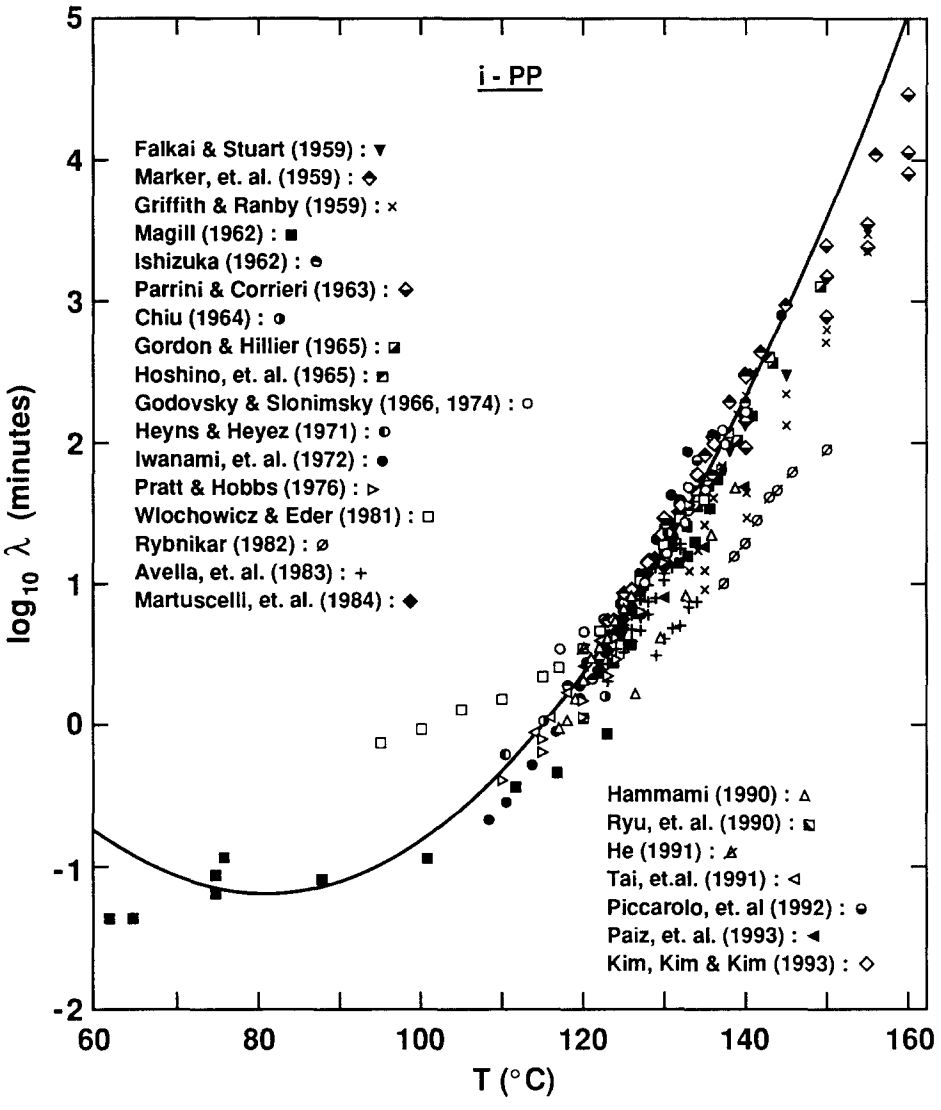

Figure 1 Cumulative data at atmospheric pressure for isothermal crystallization of isotactic polypropylene. Curve is given by equations (14) and (15)

has been made of equation (10) or of the following relation:

$$\lambda(T) \equiv k^{-1/n}(T) = \frac{t_{1/2}(T)}{(\ln 2)^{1/n}} \tag{13}$$

which follows directly from equation (1), with $\chi \equiv 1/2$ at $t \equiv t_{1/2}$. In those few cases where values for n are not given[13,30], a representative value for n of 3.0 has been taken to evaluate λ, based on equation (13). (It should be noted that $(\ln 2)^{1/n}$ is only weakly dependent upon n, changing by only 10% as n changes from 2.0 to 4.0.)

Despite scatter, the experimental results plotted in *Figure 1* clearly indicate a concentrated band which is reasonably well described by the solid curve, corresponding to

$$\ln \lambda(T) = B_1 + B_2 T + B_3 T^2 \tag{14}$$

where λ and T are in minutes and °C, respectively, and

$$B_1 = 12.28, \quad B_2 = -0.3691/°C, \quad B_3 = 0.002276/(°C)^2 \tag{15}$$

It is noted that the functional form in equation (14) has been employed often in the past, such as for chlorinated polyether[33] and PPS[34]; in addition, it is also equivalent to the Gaussian function employed by Ziabicki[35].

In observing the curve in *Figure 1*, it is noted that the minimum value of λ (i.e. fastest crystallization kinetics) occurs at ~80°C. In turn, this lies approximately midway between T_g and T_m, as would be expected[36]. For example, from ref. 37, $(T_g, T_m) \simeq (-17°C, 171°C)$, giving an average value of 77°C.

Concerning constant-cooling-rate crystallization data, *Table 2* summarizes available results from the literature[25-27,29,31,38-50] for i-PP. In this case, essentially all the data have been obtained by d.s.c. except for some light depolarizing microscopy (LDM)[25] and pressurized dilatometry[27,38,39] measurements. Shown plotted in *Figure 2* are data points from these various sources in terms of $\sigma(T)$, which has been determined from the relation

$$\sigma[T_{1/2}(\varphi)] \equiv \kappa^{1/n}[T_{1/2}(\varphi)] = (\ln 2)^{1/n} \times \varphi \tag{16}$$

which follows directly from equation (2), with $\chi \equiv 1/2$ at $T \equiv T_{1/2}$. That is, if $T_{1/2}$ is known for a given φ, then equation (16) can be used to determine $\sigma(T)$ at $T = T_{1/2}$. For those cases in *Table 2* where n is not known, a

Table 2 Summary of constant-cooling-rate crystallization data for isotactic polypropylene

Reference	Ref. no.	Method[a]	φ(°C min^{-1})	n
Leute *et al.* (1976)	38	pressurized dilatometry	0.1	–
Karl *et al.* (1977)	39	pressurized dilatometry	1.14	–
Eder and Wlochowicz (1983)	40	d.s.c.	0.5–10	2.5–3.3
Monasse and Haudin (1986)	41	d.s.c.	0.3–40	$\simeq$4.0($\lesssim$116°C) $\simeq$3.0(>122°C)
Chiang (1989)	42	d.s.c.	2.5–40	–
Hammami (1990)	25	d.s.c. LDM	5–80 2–10	2.0–3.1
Khanna (1990)	43	d.s.c.	1.25 & 40	–
Janimak and Cheng (1991)	44	d.s.c.	2.5–40	–
Ryu *et al.* (1991)	26	d.s.c.	10–30	–
He and Zoller (1991)	27	pressurized dilatometry	2.5	–
Tai *et al.* (1991)	29	d.s.c.	2.5–40	–
Kim *et al.* (1991)	45	d.s.c.	0.5–16	2.1–2.5
Mitsuishi *et al.* (1991)	46	d.s.c.	3	–
Bozarth *et al.* (1991)	47	d.s.c.	5–80	–
Jou (1992)	48	d.s.c.	0.1–70	2.2–3.3($\gtrsim$115°C) 2.4–4.6($\lesssim$110°C)
Paiz *et al.* (1993)	31	d.s.c.	5–20	–
Chan *et al.* (1993)	49	d.s.c.	2.5–20	–
Narh and Roa (1993)	50	d.s.c.	5–20	2.7–3.1

[a] See footnote to *Table 1* for abbreviations

representative value for n of 3.0 has been used in calculating the points in *Figure 2*, based upon equation (16). As in the case of equation (13), it is seen that the calculation of $\sigma(T)$ based upon equation (16) is only weakly dependent upon the value of n.

Despite scatter in the experimental results plotted in *Figure 2*, there is an evident concentrated band of results. This band is well represented by the solid curve in *Figure 2*, which has been generated based upon equation (11) with $\lambda(T)$ given by equations (14) and (15), corresponding to the curve fit of the isothermal crystallization data in *Figure 1*. Specifically, a Runge–Kutta procedure has been used to generate $\sigma(T)$ numerically from $\lambda(T)$, starting at sufficiently large T where σ and λ^{-1} are vanishingly small. Taken together, the results from *Figures 1* and *2* indicate a self-consistency between the bulk of the available isothermal and constant-cooling-rate crystallization data for i-PP, as well as a validation of the present approach for modelling the crystallization kinetics. These results for i-PP will be discussed further after first considering similar results for PET in the next section.

APPLICATION TO PET

For the case of PET, *Table 3* lists available experimental sources from the literature[5,20,51–67] based upon various methods, as indicated. Shown plotted in *Figure 3* are data points from these various sources in terms of $\lambda(T)$, where use has been made of equations (10) or (13), with n again taken to be 3.0 when unavailable from the given source[54,57,59,63]. Unlike the corresponding isothermal crystallization data for i-PP in *Figure 1*, it is noted that the results in *Figure 3* are fairly uniformly scattered with no evident band of concentration. In particular, the curve in *Figure 3* corresponds to the best fit of the cumulative data in terms of the quadratic functional form in equation (14), with

$$B_1 = 25.04, \quad B_2 = -0.2903/°C, \quad B_3 = 8.434 \times 10^{-4}/(°C)^2 \tag{17}$$

Accordingly, the minimum value of λ based upon this fit occurs at $\sim$172°C. By comparison, from ref. 37, (T_g, T_m) $\simeq$(74°C, 257°C), giving an average value of $\sim$166°C. Hence, even though the absolute value of $\lambda(T)$ is highly scattered amongst the cumulative data in *Figure 3*, the temperature where λ reaches its minimum value does seem to be quite well defined and correlates reasonably well with the average of T_g and T_m.

Concerning non-isothermal crystallization data for PET, the available sources in the literature are much more limited, as listed in *Table 4*. In terms of $\sigma(T)$, the corresponding data points from these sources are shown in *Figure 4*. As in the case of *Figure 3*, the results in *Figure 4* indicate substantial scatter amongst the various datasets. Accordingly, the situation for PET is distinctly different from that for i-PP, where the cumulative isothermal and non-isothermal crystallization data in *Figures 1* and *2* show evident concentrated bands, which have been shown to be related to each other through the use of equation (11). In contrast, in dealing with PET it becomes necessary to deal separately with each individual resin.

As an illustration, *Figure 5* shows the isothermal crystallization data[66] for resins A and B, where the curves

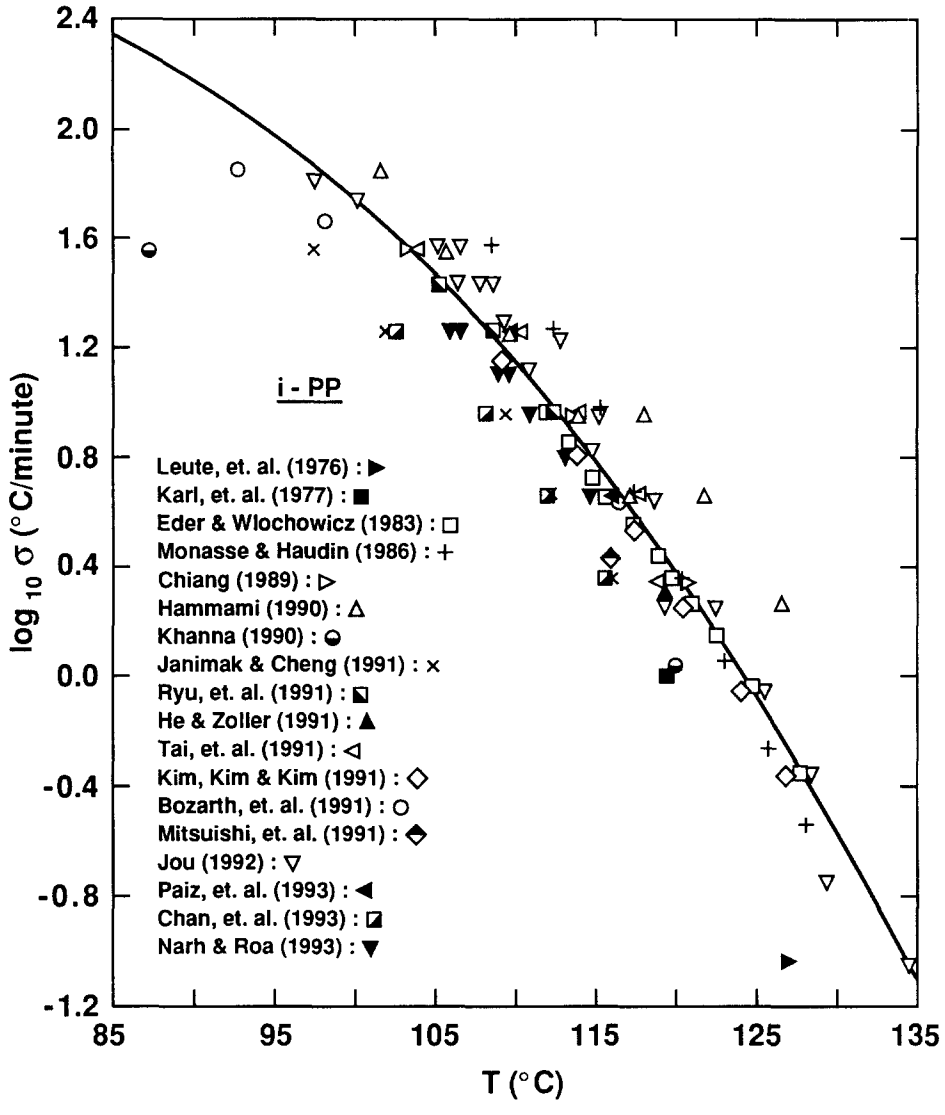

Figure 2 Cumulative data at atmospheric pressure for constant-cooling-rate crystallization of i-PP in terms of $\sigma(T)$. Results from Leute *et al.*[38], Karl *et al.*[39] and He and Zoller[27] are based upon high-pressure data extrapolated to zero (gauge) pressure as documented in the Appendix. Curve has been generated from curve in *Figure 1* by making use of equation (11)

are corresponding best fits based upon equation (14) subject to $T_{min} = 172°C$ (based upon cumulative results in *Figure 3*), namely for resin A

$$B_1 = 28.92, \quad B_2 = -0.3537/°C, \quad B_3 = 1.028 \times 10^{-3}/(°C)^2 \tag{18}$$

and for resin B

$$B_1 = 26.13, \quad B_2 = -0.2983/°C, \quad B_3 = 8.672 \times 10^{-4}/(°C)^2 \tag{19}$$

Based upon these respective fits for $\lambda(T)$, $\sigma(T)$ has been generated numerically by applying a Runge–Kutta procedure to equation (11). The resulting curves are plotted in *Figure 6* together with the independently obtained non-isothermal data points[66]. For both resins, it is seen that the curves describe the data points extremely well. This serves to confirm the consistency of the isothermal and non-isothermal crystallization data from Douillard *et al.*[66] as well as the viability of the present modelling procedure.

As a further illustration, *Figure 7* shows the isothermal crystallization data from Chan and Isayev[67]. In particular, the low-temperature data points in *Figure 7* correspond to 'cold crystallization', in which the initially molten polymer was thermally quenched (amorphously) and then heated up to the indicated temperature. The solid curve corresponds to the best fit of the data (omitting the somewhat anomalous point at 211°C) based upon equation (14), namely

$$B_1 = 34.27, \quad B_2 = -0.4108/°C, \quad B_3 = 1.227 \times 10^{-3}/(°C)^2 \tag{20}$$

On the other hand, the dashed curve is the corresponding best fit subject to fixing $\lambda_{min} = 1.00$ min (as will be used in discussing the non-isothermal results below), namely

$$B_1 = 33.33, \quad B_2 = -0.3984/°C, \quad B_3 = 1.191 \times 10^{-3}/(°C)^2 \tag{21}$$

Shown in *Figure 8* are corresponding points from the constant-cooling-rate and constant-heating-rate crystallization data of Chan and Isayev[67] where the curves have been generated based upon equation (11) with $\lambda(T)$ given by either equations (14) and (20) or equations (14) and (21), corresponding to the respective solid and dashed curves in *Figure 7*. In particular, it is noted that the solid cooling curve (C in *Figure 8*) describes the corresponding

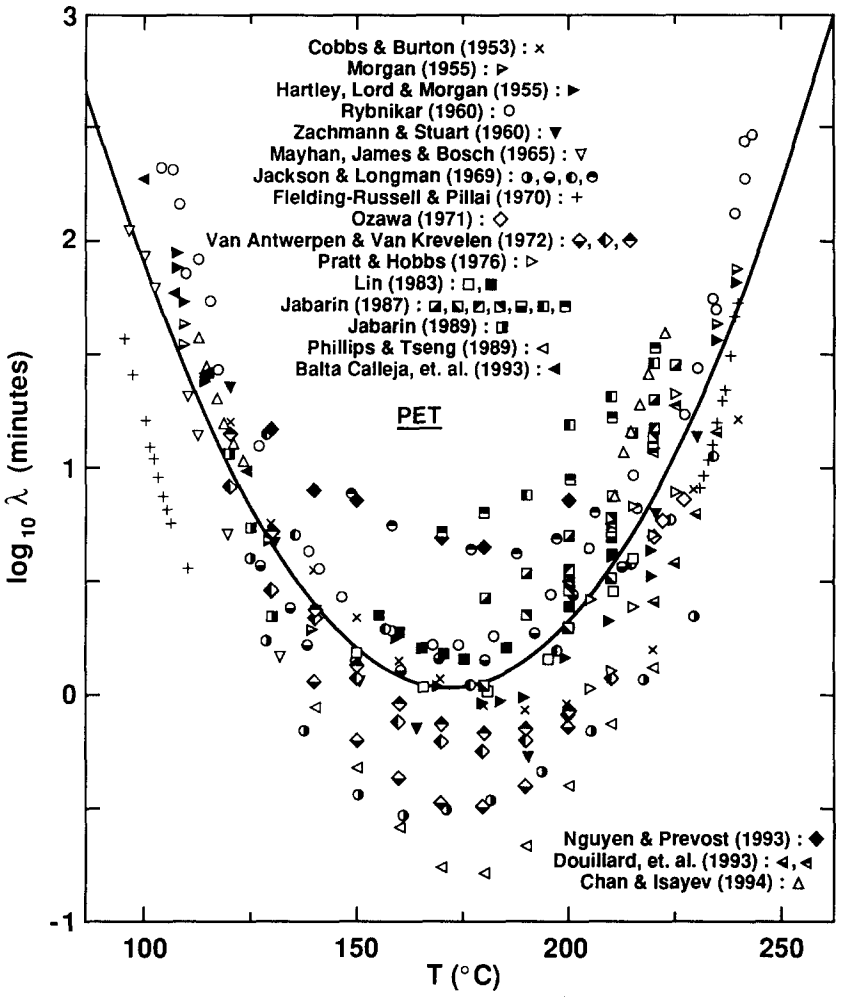

Figure 3 Cumulative data for isothermal crystallization of PET. Curve corresponds to best fit given by equations (14) and (17)

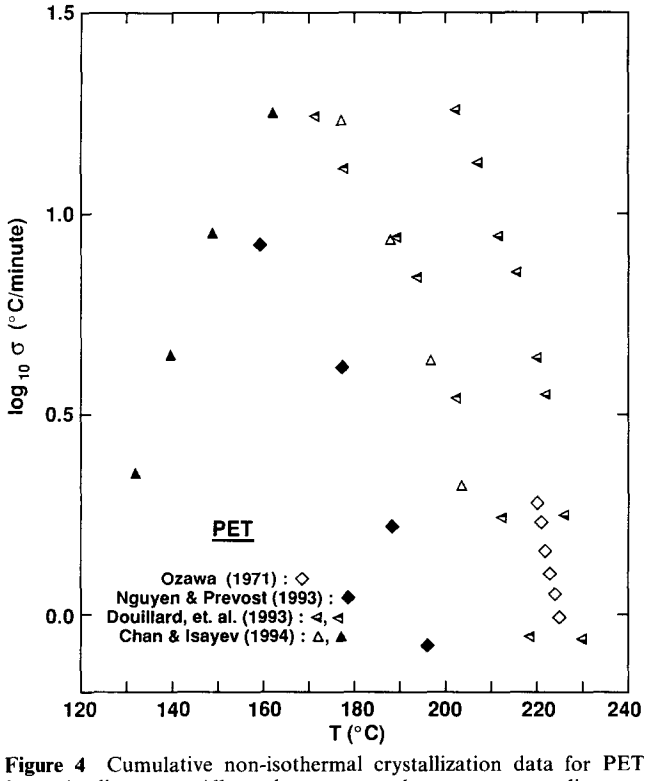

Figure 4 Cumulative non-isothermal crystallization data for PET from the literature. All results correspond to constant-cooling-rate measurements except for constant-heating-rate data (▲) from Chan and Isayev[67]

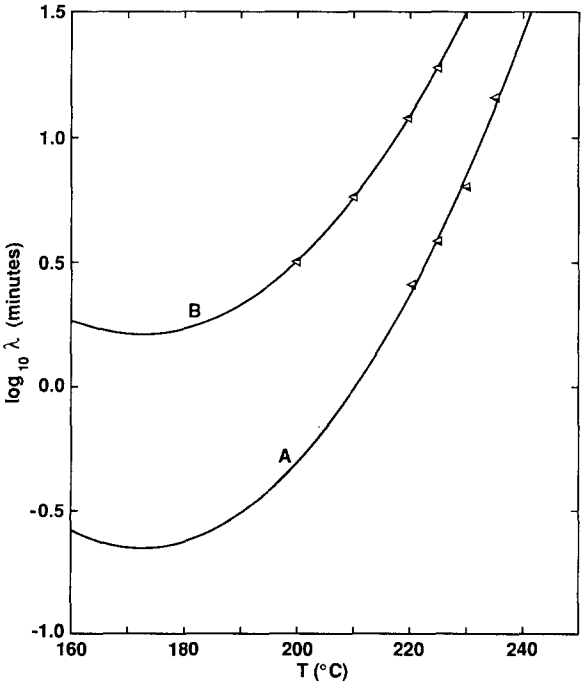

Figure 5 Isothermal crystallization data points for PET from Douillard *et al.*[66] for resins A and B. Curves are corresponding best fits given by equations (14) and (18) for A and equations (14) and (19) for B

Table 3 Summary of isothermal crystallization data for PET

Reference	Ref. no.	Method[a]	T(°C)	n
Cobbs and Burton (1953)	51	i.r.s.	120–240	1.3–3.1
Morgan (1955)	52	d.g.c.	110–140	2
		dilatometry	110, 236, 240	2, 4, 4
Hartley *et al.* (1955)	53	d.g.c.	108–240	2–4
		dilatometry	108, 115, 235	3, 2, 4
Zachmann and Stuart (1960)	54	density	120–230	–
Rybnikar (1960)	55	d.g.c. and dilatometry	104–244	2–4
Mayhan *et al.* (1965)	56	spectrometry	96–132	1.0–1.5
Jackson and Longman (1969)	57	LDM	124–235	–
Fielding-Russell and Pillai (1970)	58	d.s.c.	95–110	4.4–4.9
			231–240	3.4–4.0
Ozawa (1971)	5	d.s.c.	220–227	3.4–3.6
Van Antwerpen and Van Krevelen (1972)	59	LDM	120–205	–
Pratt and Hobbs (1976)	20	d.s.c.	200–225	3.0–3.2
		LDM	205–225	2.9–3.5
Lin (1983)	60	d.s.c.	150–215	≈2.9
Jabarin (1987)	61	d.s.c.	170–225	2.0–3.3
Jabarin (1989)	62	LDM	115–130	2.3–2.6
Phillips and Tseng (1989)	63	optical transmission and light scattering	140–220	–
Balta Calleja *et al.* (1993)	64	microhardness	110–117	2.7–3.3
Nguyen and Prevost (1993)	65	d.s.c.	130–200	1.8–2.8
Douillard *et al.* (1993)	66	d.s.c.	200–235	2.6–2.8
Chan and Isayev (1993)	67	d.s.c.	113–123	2.5–2.8
			211–223	2.3–2.5

[a] D.g.c., density-gradient column; see footnote to *Table 1* for other abbreviations

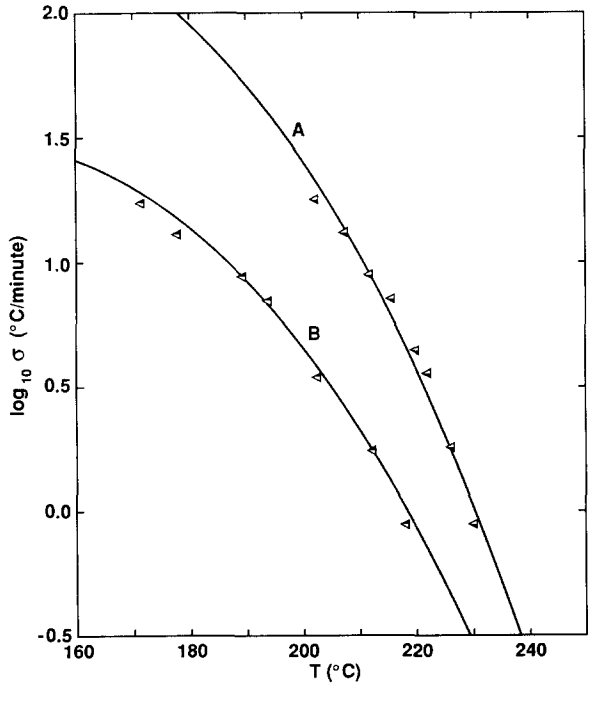

Figure 6 Constant-cooling-rate crystallization data points for PET from Douillard *et al.*[66] for resins A and B. Curves A and B have been generated from the respective curves in *Figure 5* via equation (11)

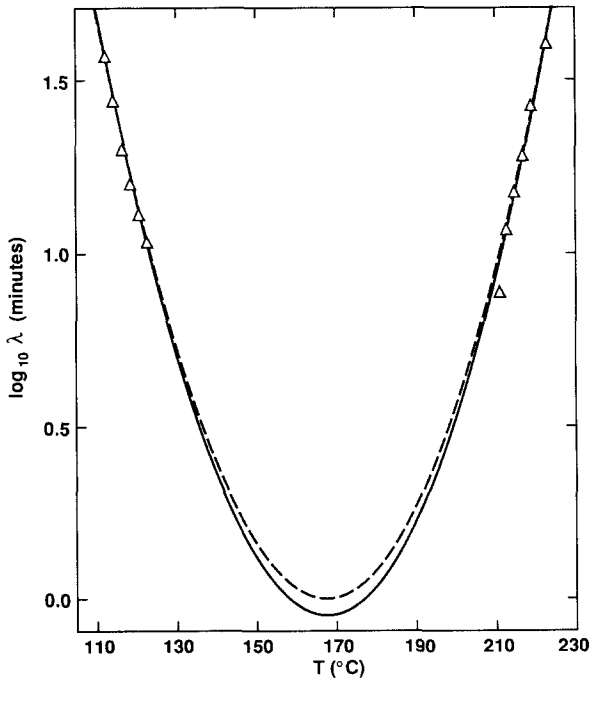

Figure 7 Isothermal crystallization data for PET from Chan and Isayev[67]. Solid and dashed curves are fits corresponding to equations (14) and (20) and equations (14) and (21), respectively

Table 4 Summary of non-isotherm crystallization data[5,65 67] for PET

Reference	Ref. no.	Method	φ(C min^{-1})[a]	n
Ozawa (1971)	5	d.s.c.	1, 2, 4	~4.0
Nguyen and Prevost (1993)	65	d.s.c.	1, 2, 5, 10	1.6–2.3
Douillard *et al.* (1993)	66	d.s.c.	1, 2, 4, 5, 8, 10, 15, 20	2.5–2.9
Chan and Isayev (1994)	67	d.s.c.	2.5, 5, 10, 20	2.0–2.5
			−2.5, −5, −10, −20	3.0–3.5

[a] Negative values correspond to constant *heating* rate

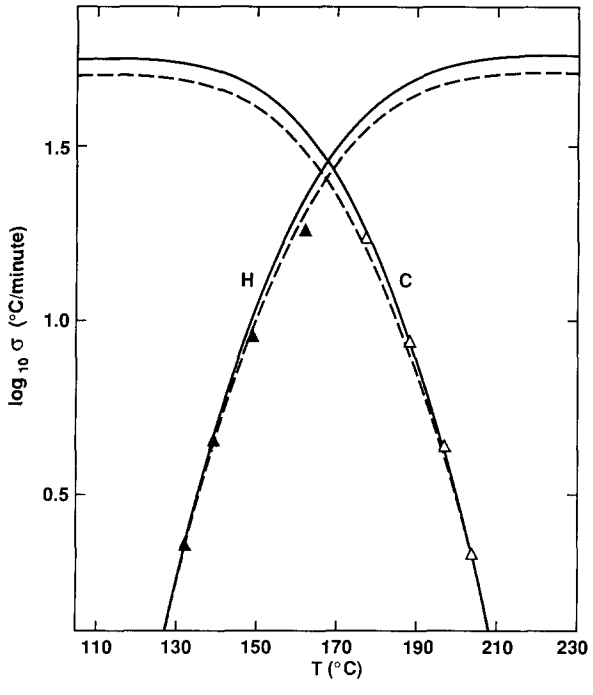

Figure 8 Constant-cooling-rate (△) and constant-heating-rate (▲) crystallization data for PET from Chan and Isayev[67]. Solid and dashed curves have been generated from the corresponding curves in *Figure 7* by using equation (11), with the minus sign omitted in the heating case (curve H)

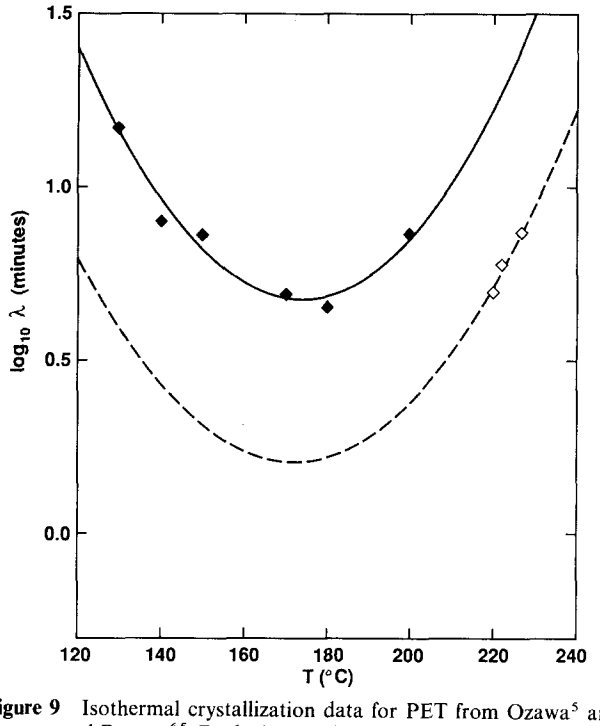

Figure 9 Isothermal crystallization data for PET from Ozawa[5] and Nguyen and Prevost[65]. Dashed and solid curves are corresponding fits given by equations (14) and (22) and equations (14) and (23), respectively

data (open triangles) very well, whereas the solid heating curve (H in *Figure 8*) tends to lie higher than the corresponding data (solid triangles), particularly the points at 149°C and 162°C which correspond to the higher heating rates of 10 and 20°C min^{-1}, respectively. It is noted, however, that the underlying isothermal data points in *Figure 7* do not include the rather extensive intermediate temperature range between 125°C and 210°C. Accordingly, it is possible to shift the fit in this intermediate range without compromising the fit of the actual data points. This has been done in the case of the dashed curve in *Figure 7*, where λ_{min} has been specified as 1.00 min, thereby shifting the curve up in the intermediate range. This upward shift in λ corresponds to slower kinetics, which translates into a downward shift in the dashed curves in *Figure 8*. In turn, the resulting dashed curves in *Figure 8* are seen to describe the heating and cooling data equally well. Hence, the results in *Figures 7* and *8* serve as a check on the self-consistency between the isothermal and non-isothermal crystallization data of Chan and Isayev[67], while substantiating the viability of the present modelling.

Concerning the remaining two sources listed in *Table 4*, *Figure 9* plots results corresponding to the isothermal crystallization measurements of Ozawa[5] and of Nguyen and Prevost[65]. The dashed curve in *Figure 9* is the best fit in terms of equation (14) of the limited data from Ozawa, subject to the constraint that $T_{min} = 172$°C, namely

$$B_1 = 15.26, \quad B_2 = -0.1719/°C, \quad B_3 = 4.996 \times 10^{-4}/(°C)^2 \tag{22}$$

whereas the solid curve is the corresponding best fit of the six solid points in *Figure 9*, namely

$$B_1 = 19.21, \quad B_2 = -0.2034/°C, \quad B_3 = 5.856 \times 10^{-4}/(°C)^2 \tag{23}$$

When these results for $\lambda(T)$ are then used to generate $\sigma(T)$ based upon numerical integration of equation (11), we get the curves shown in *Figure 10*. In both instances, the corresponding experimental results[5,65] are seen to lie decidedly below the respective curves. That is, the present modelling indicates that the constant-cooling-rate crystallization data[5,65] correspond to slower kinetics than the respective isothermal crystallization data. Accordingly, comparison of the results in *Figures 9* and *10* indicates

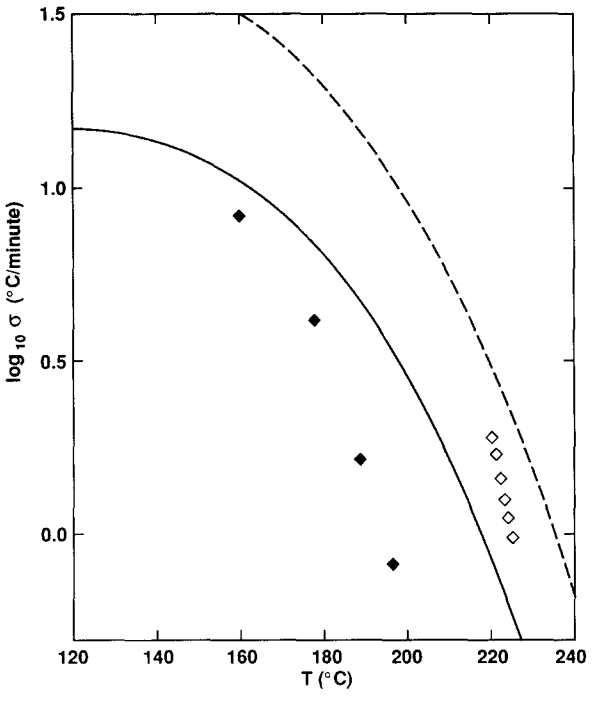

Figure 10 Constant-cooling-rate data from Ozawa[5] and Nguyen and Prevost[65]. Dashed and solid curves have been generated from the corresponding curves in *Figure 9* via equation (11)

that either the present modelling is inappropriate or else the two types of measurements from each of these sources are inconsistent. Given the ability of the present modelling to describe the more extensive data from the other sources[66,67] very well, it seems that the results in *Figures 9* and *10* draw into question the reliability of the underlying datasets[5,65].

DISCUSSION

In observing the experimental results such as in *Figures 1–4*, one concern is whether the evident scatter is a reflection of significant variations in the actual crystallization kinetics of such polymers or rather a result of experimental uncertainties or inaccuracies. In this regard, it is instructive to refer to the data of Hammami[25], which include isothermal and constant-cooling-rate data for i-PP based upon both the d.s.c. and LDM methods. Referring to his results in *Figure 1*, it is noted that his five data points that lie low are all based upon LDM measurements, whereas his remaining points in *Figure 1* all lie within the concentrated band and are based upon d.s.c. data. Similarly, his three data points that lie anomalously high in *Figure 2* are based upon LDM whereas the remaining five points lie within the concentrated band and are based upon d.s.c. That is, for both the isothermal and constant-cooling-rate cases, the LDM measurements of Hammami indicate faster kinetics (i.e. smaller λ in *Figure 1* and larger σ in *Figure 2*) than the d.s.c. measurements, all for the same commercial-grade polymer. Accordingly, at least for the data points of Hammami[25], it is clear that the associated large scatter in *Figures 1* and *2* is not due to variations in the actual crystallization kinetics but rather due to uncertainties or inaccuracies in the actual measurements. As a further case in point, it is noted that Pratt and Hobbs[20] obtained isothermal crystallization data for both i-PP and PET and used both d.s.c. and LDM techniques in each case. For i-PP, the two types of measurement were found to agree quite well, whereas for PET (as well as poly(butylene terephthalate)), the LDM data indicated systematically faster kinetics than those based upon d.s.c. measurements. Accordingly, it is again seen that the scatter amongst the reported data, in this case for PET[20], is at least partially due to experimental uncertainties.

On the other hand, the contrast between *Figures 1* and *3*, in which a concentrated band is evident in the former but not in the latter, is another matter. For PET, several investigators[57,59–61] have studied the effect of molecular weight and found that the kinetics get slower with increasing molecular weight, although some results[59] suggest that the kinetics become independent of molecular weight as the latter becomes sufficiently large (specifically, when $\bar{M}_n \gtrsim 60\,000$). Another factor is the catalyst which, for the case of PET, has been found[57,61] to have an effect upon the kinetics at least as significant as that of molecular weight. For the i-PP case, we have typically considered commercial grades for which the molecular weight may be sufficiently high (based upon the results of ref. 59 for PET) to have little effect on the kinetics. Curiously, however, some investigators[13,44] dealing with i-PP fractions have found that the kinetics get faster with increasing molecular weight (in contrast to the results[57,59–61] for PET); when reporting experimental results for such i-PP fractions, we have used the data[44] corresponding to the higher molecular weight.

As a further illustration of the present correlation for i-PP, *Figure 11* shows a plot for the constant-cooling-rate case in terms of the more typical $T_{1/2}$ *versus* φ, where the curve has been generated from the curve in *Figure 2*, as indicated. In effect, this figure is an alternative presentation of *Figure 2*; accordingly, it is not surprising that the curve again represents the bulk of the data fairly well.

Proceeding one step further, the symbols in *Figure 12* correspond to experimental results for i-PP under constant cooling rate in terms of $T_{1/10}$–$T_{9/10}$. That is, the ordinate in *Figure 12* represents the temperature band over which χ changes from 10% to 90% at fixed φ. The curves in *Figure 12* are based upon the following relationships, which follow from equation (2) in the same manner as equation (16), namely

$$\sigma[T_{1/10}(\varphi)] \equiv \kappa^{1/n}[T_{1/10}(\varphi)] = [\ln(10/9)]^{1/n} \times \varphi \quad (24)$$

and

$$\sigma[T_{9/10}(\varphi)] \equiv \kappa^{1/n}[T_{9/10}(\varphi)] = [\ln(10)]^{1/n} \times \varphi \quad (25)$$

Both the data and curves are seen to indicate that $T_{1\,10}$–$T_{9\,10}$ increases with φ. Further, the data are seen to exhibit a concentrated band which, relative to the curves, suggests a representative value for n of ~ 2.7. (Note that only one curve has been shown in *Figure 11* since $T_{1/2}(\varphi)$ is only weakly dependent on n, the $(\ln 2)^{1/n}$ factor in equation (16) changing by only 10% as n changes from 2 to 4.)

In observing the results at the higher φ in *Figure 12*, it is noted that there is a tendency for the experimental results to upturn faster than the curves. In order to investigate this behaviour further, *Figure 13* shows results analogous to *Figure 12* but now in terms of $T_{1/10}$–$T_{2/3}$ *versus* φ, where use has been made of the relation

$$\sigma[T_{2/3}(\varphi)] \equiv \kappa^{1/n}[T_{2/3}(\varphi)] = (\ln 3)^{1/n} \times \varphi \quad (26)$$

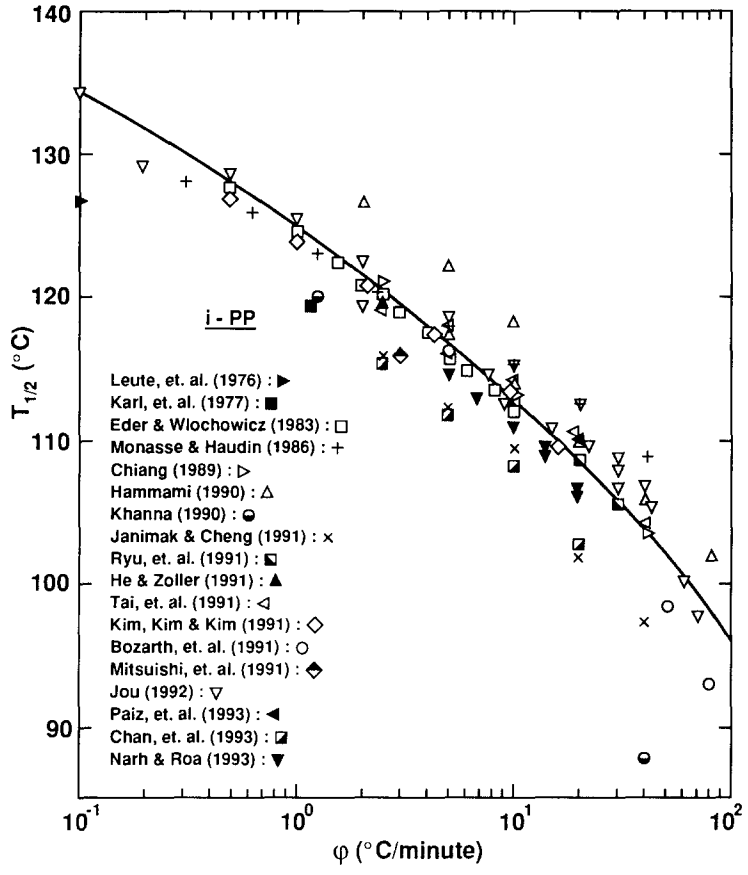

Figure 11 Results for constant-cooling-rate crystallization of i-PP in terms of $T_{1/2}$ *versus* φ. Curve has been generated from equation (16) with $\sigma(T)$ based on curve in *Figure 2* and n assumed to be 3.0

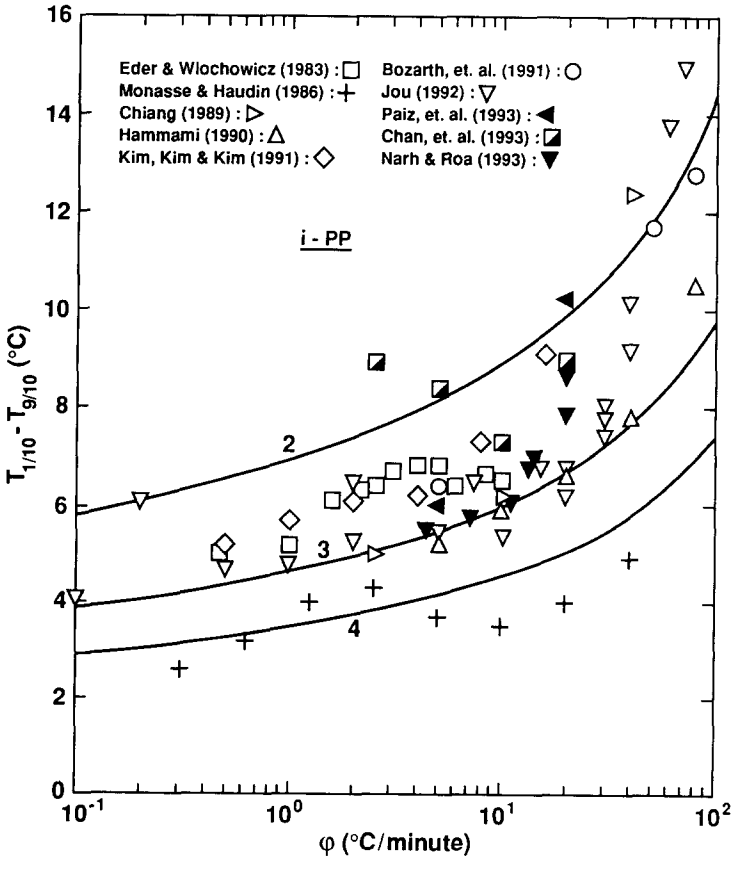

Figure 12 Results for constant-cooling-rate crystallization of i-PP in terms of $T_{1/10}-T_{9/10}$ *versus* φ. Curves have been generated from equations (24) and (25) with $\sigma(T)$ based upon curve in *Figure 2* and n taken as 2, 3 or 4, as indicated

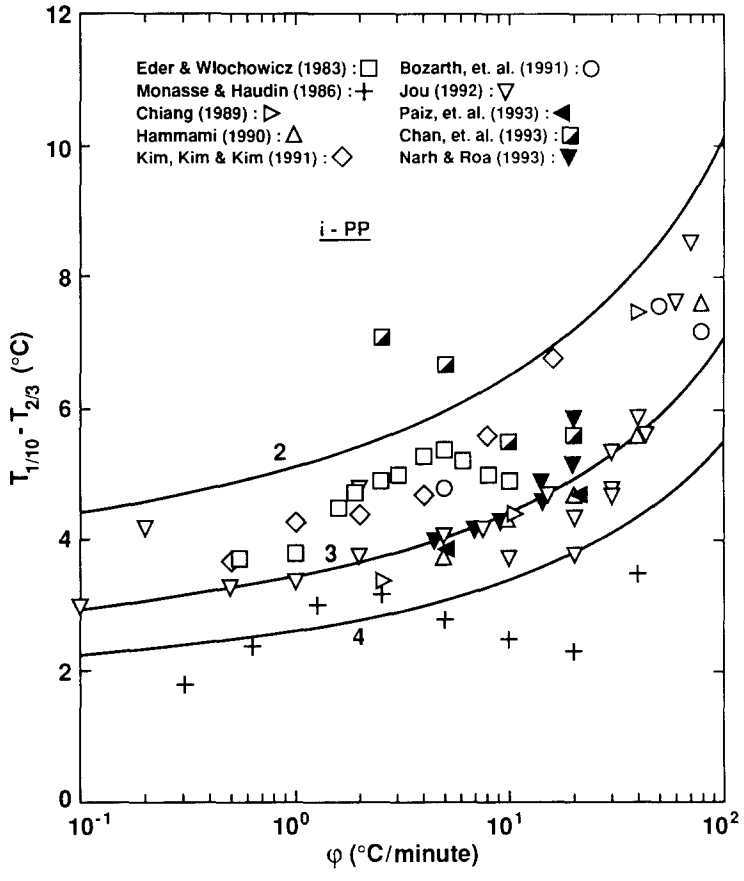

Figure 13 As for *Figure 12* but for $T_{1/10}$–$T_{2/3}$ *versus* φ and with curves generated from equations (24) and (26)

which also follows from equation (2). Unlike *Figure 12*, the high φ results in *Figure 13* are seen to be reasonably compatible with the lower φ results and the trends of the curves, with $n \approx 2.7$ being a representative value for the cumulative results. Accordingly, based upon the results in *Figures 1, 2* and *13*, it appears that the present modelling describes the crystallization kinetics of i-PP reasonably well, at least up to $\chi \approx 2/3$ and for $\varphi \lesssim 10^2$°C min^{-1}. In addition, the modelling can be extended reasonably well to elevated pressure, as is documented in the Appendix.

ACKNOWLEDGEMENTS

This work has been supported by the Cornell Injection Molding Program. Special thanks are due to Dr James M. O'Reilly of Eastman Kodak Research Laboratories for bringing the paper by Passaglia and Martin to the author's attention.

REFERENCES

1 Nakamura, K., Watanabe, T., Katayama, K. and Amano, T. *J. Appl. Polym. Sci.* 1972, **16**, 1077
2 Nakamura, K., Watanabe, T., Katayama, K. and Amano, T. *J. Appl. Polym. Sci.* 1973, **17**, 1031
3 Avrami, M. *J. Chem. Phys.* 1939, **7**, 1103
4 Avrami, M. *J. Chem. Phys.* 1940, **8**, 212
5 Ozawa, T. *Polymer* 1971, **12**, 150
6 Falkai, B. V. and Stuart, H. A. *Kolloid Z.* 1959, **162**, 138
7 Marker, L., Hay, P. M., Tilley, G. P., Early, R. M. and Sweeting, O. J. *J. Polym. Sci.* 1959, **38**, 33
8 Griffith, J. H. and Ranby, B. G. *J. Polym. Sci.* 1959, **38**, 107
9 Magill, J. H. *Polymer* 1962, **3**, 35
10 Ishizuka, O. *Kogyo Kagaku Zasshi* 1962, **65**, 247
11 Ishizuka, O. and Koyama, K. *Polymer* 1977, **18**, 913
12 Parrini, P. and Corrieri, G. *Makromol. Chem.* 1963, **62**, 83
13 Chiu, J. *Anal. Chem.* 1964, **36**, 2058
14 Gordon, M. and Hillier, I. H. *Polymer* 1965, **6**, 213
15 Hoshino, S., Meinecke, E., Powers, J. and Stein, R. S. *J. Polym. Sci., Part A* 1965, **3**, 3041
16 Godovsky, Y. K. and Slonimsky, G. L. *Vysokomol. Soedin* 1966, **8**, 403
17 Heyns, H. and Heyez, S. *Proc. Third Int. Conf. Therm. Anal.* 1971, **3**, 341
18 Iwanami, T., Takai, R. and Kaneko, R. *Kobunshi Kagaku* 1972, **29**, 139
19 Godovsky, Y. K. and Slonimsky, G. L. *J. Polym. Sci., Polym. Phys. Edn* 1974, **12**, 1053
20 Pratt, C. F. and Hobbs, S. Y. *Polymer* 1976, **17**, 12
21 Wlochowicz, A. and Eder, M. *Polymer* 1981, **22**, 1285
22 Rybnikar, F. *J. Appl. Polym. Sci.* 1982, **27**, 1479
23 Avella, M., Martuscelli, E. and Pracella, M. *J. Therm. Anal.* 1983, **28**, 237
24 Martuscelli, E., Pracella, M., Volpe, G. D. and Greco, P. *Makromol. Chem.* 1984, **185**, 1041
25 Hammami, A. MS Thesis, University of Tennessee, Knoxville, 1990
26 Ryu, S. H., Gogos, C. G. and Xanthos, M. *SPE ANTEC Tech. Papers* 1991, **37**, 886
27 He, J. and Zoller, P. *SPE ANTEC Tech. Papers* 1991, **37**, 1723
28 He, J. Internal Report, Department of Mechanical Engineering, University of Colorado at Boulder, 1991
29 Tai, H.-J., Chiu, W.-Y., Chen, L.-W. and Chu, L.-H. *J. Appl. Polym. Sci.* 1991, **42**, 3111
30 Piccarolo, S., Saiu, M., Brucato, V. and Titomanlio, G. *J. Appl. Polym. Sci.* 1992, **46**, 625
31 Paiz, R., Nigam, P. and Wesson, R. D. *SPE ANTEC Tech. Papers* 1993, **39**, 242
32 Kin, C. Y., Kim, Y. C. and Kim, S. C. *Polym. Eng. Sci.* 1993, **33**, 1445
33 Sifleet, W. L., Dinos, N. and Collier, J. R. *Polym. Eng. Sci.* 1973, **13**, 10
34 Jog, J. P. and Nadkarni, V. M. *J. Appl. Polym. Sci.* 1985, **30**, 997

35 Ziabicki, A. 'Fundamentals of Fibre Formation', Wiley, London, 1976
36 Van Krevelen, D. W. *Chimia* 1978, **32**, 279
37 Brandrup, J. and Immergut, E. H. 'Polymer Handbook', 3rd edn, Wiley, New York, 1989
38 Leute, U., Dollhopf, W. and Liska, E. *Colloid Polym. Sci.* 1976, **254**, 237
39 Karl, V. H., Asmussen, F. and Ueberreiter, K. *Makromol. Chem.* 1977, **178**, 2037
40 Eder, M. and Wlochowicz, A. *Polymer* 1983, **24**, 1593
41 Monasse, B. and Haudin, J. M. *Colloid Polym. Sci.* 1986, **264**, 117
42 Chiang, H. H. PhD Thesis, Cornell University, Ithaca, NY, 1989
43 Khanna, Y. P. *Polym. Eng. Sci.* 1990, **30**, 1615
44 Janimak, J. J. and Cheng, S. Z. D. *J. Polym. Eng.* 1991, **10**, 21
45 Kim, Y. C., Kim, C. Y. and Kim, S. C. *Polym. Eng. Sci.* 1991, **31**, 1009
46 Mitsuishi, K., Ueno, S., Kodama, S. and Kawasaki, H. *J. Appl. Polym. Sci.* 1991, **43**, 2043
47 Bozarth, M. J., Allen, V. L., Millar, S. A., Gregors, R. D., Klinger, K. A. and Galamkos, A. F. Personal communication, Himont R & D Center, Wilmington, DE, 1991
48 Jou, W.-S. Personal communication, Cornell Injection Molding Program, 1992
49 Chan, T. W., Shimojo, K. and Isayev, A. I. *SPE ANTEC Tech. Papers* 1993, **39**, 1032
50 Narh, K. A. and Roa, E. Personal communication, Cornell Injection Molding Program, 1993
51 Cobbs, W. H. and Burton, R. L. *J. Polym. Sci.* 1953, **10**, 275
52 Morgan, L. B. *Phil. Trans. R. Soc. London (Series A)* 1955, **247**, 13
53 Hartley, F. D., Lord, F. W. and Morgan, L. B. *Phil. Trans. R. Soc. London (Series A)* 1955, **247**, 23
54 Zachmann, H. G. and Stuart, H. A. *Makromol. Chem.* 1960, **41**, 131
55 Rybnikar, F. *Collection Czech. Chem. Commun.* 1960, **25**, 1529
56 Mayhan, K. G., James, W. J. and Bosch, W. *J. Appl. Polym. Sci.* 1965, **9**, 3605
57 Jackson, J. B. and Longman, G. W. *Polymer* 1969, **10**, 873
58 Fielding-Russell, G. S. and Pillai, P. S. *Makromol. Chem.* 1970, **135**, 263
59 Van Antwerpen, F. and Van Krevelen, D. W. *J. Polym. Sci. (Phys.)* 1972, **10**, 2423
60 Lin, C. C. *Polym. Eng. Sci.* 1983, **23**, 113
61 Jabarin, S. A. *J. Appl. Polym. Sci.* 1987, **34**, 85
62 Jabarin, S. A. *Polym. Eng. Sci.* 1989, **29**, 1259
63 Phillips, P. J. and Tseng, H. T. *Macromolecules* 1989, **22**, 1649
64 Balta Calleja, F. J., Santa Cruz, C. and Asano, T. *J. Polym. Sci. (Part B: Polym. Phys.)* 1993, **31**, 557
65 Nguyen, K. T. and Prevost, G. *SPE ANTEC Tech. Papers* 1993, **39**, 245
66 Douillard, A., Dumazet, Ph., Chabert, B. and Guillet, J. *Polymer* 1993, **34**, 1702
67 Chan, T. W. and Isayev, A. I. *Polym. Eng. Sci.* 1994, **34**, 461
68 Nelder, J. A. and Mead, R. *Computer J.* 1965, **7**, 308
69 Fortune, L. R. and Malcolm, G. N. *J. Phys. Chem.* 1960, **64**, 934
70 Baer, E. and Kardos, J. L. *J. Polym. Sci. (Part A)* 1965, **3**, 2827
71 Leute, U., Dollhopf, W. and Liska, E. *Colloid Polym. Sci.* 1978, **356**, 914
72 Passaglia, E. and Martin, G. M. *J. Res. (NBS)* 1964, **68A**, 273

APPENDIX

Pressure dependence for i-PP

As noted in *Tables 1* and *2*, crystallization data for i-PP at elevated pressures are available in terms of isothermal and constant-cooling-rate measurements by He and Zoller[27] as well as constant-cooling-rate data by Leute *et al.*[38] and Karl *et al.*[39]. Shown plotted in *Figure 14* are the isothermal data[27] points expressed in terms of $\lambda(T,p)$. In addition, curve 0 in *Figure 14* corresponds to the correlation at zero (gauge) pressure from *Figure 1*, as defined by equations (14) and (15). Based upon comparison of the symbols and curve 0 in *Figure 14*, it appears that the pressure-dependence effect might be modelled, in first approximation, in terms of an effective shift in the temperature scale. That is, equation (14) might be extended to elevated pressures as follows:

$$\ln \lambda(T,p) = B_1 + B_2\tilde{T} + B_3\tilde{T}^2 \tag{27}$$

where

$$\tilde{T} \equiv T - T_{\text{shift}}(p) \tag{28}$$

and

$$T_{\text{shift}}(p) = B_4 p + B_5 p^2 \tag{29}$$

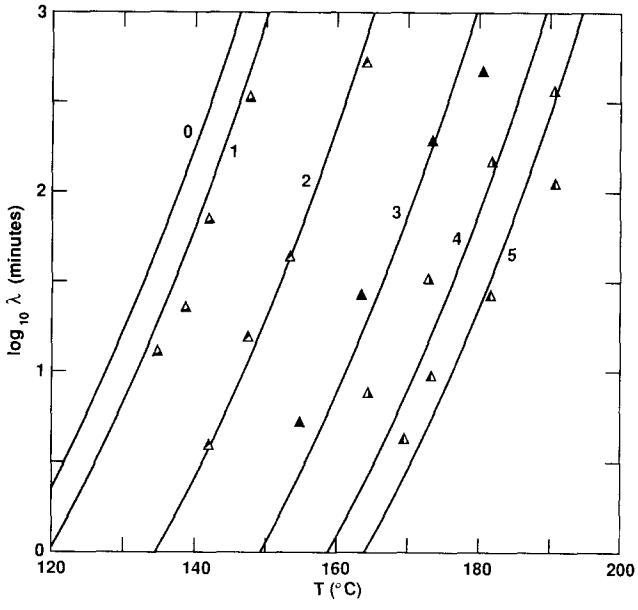

Figure 14 Isothermal crystallization data points for i-PP from He and Zoller[27] at pressures of 100 to 2000 bar. Curve 0 corresponds to the correlation at atmospheric pressure given by the curve in *Figure 1* whereas curves 1–5 correspond to pressures of 100, 500, 1000, 1500 and 2000 bar, respectively, based upon equations (15) and (27)–(30)

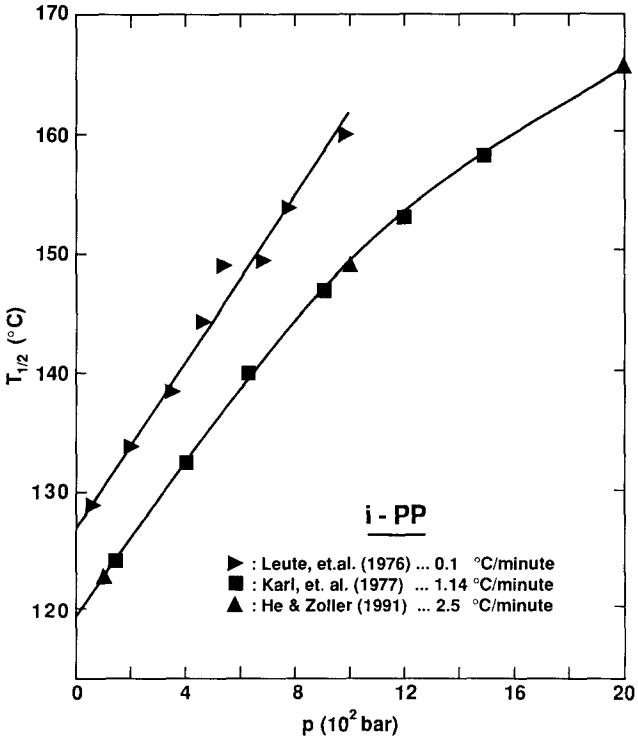

Figure 15 Results for $T_{1/2}(p)$ from constant-cooling-rate data for i-PP at elevated pressure[27,38,39]. Curves are graphical fits

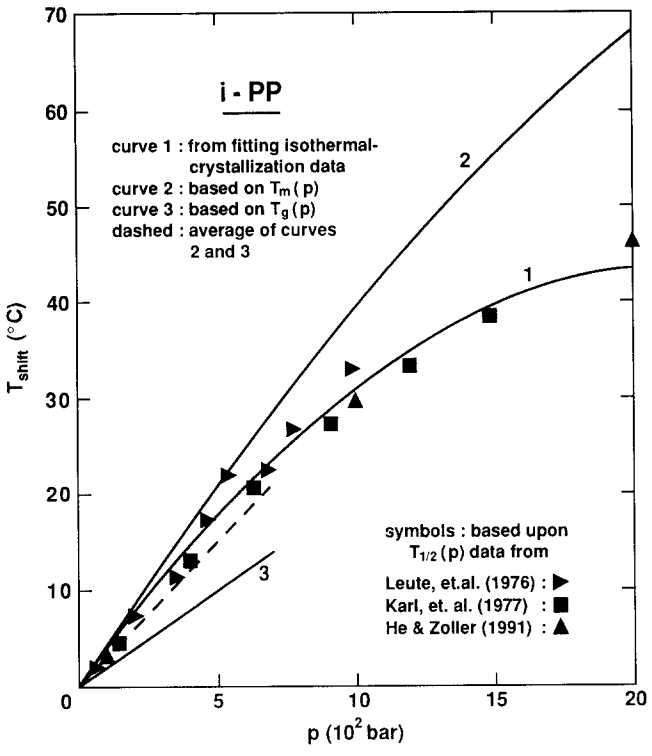

Figure 16 Results for $T_{shift}(p)$ where symbols are based upon respective results from *Figure 15*; curve 1 is based upon equations (29) and (30) whereas curves 2 and 3 are based upon respective results for $T_m(p)$ and $T_g(p)$, as documented in text

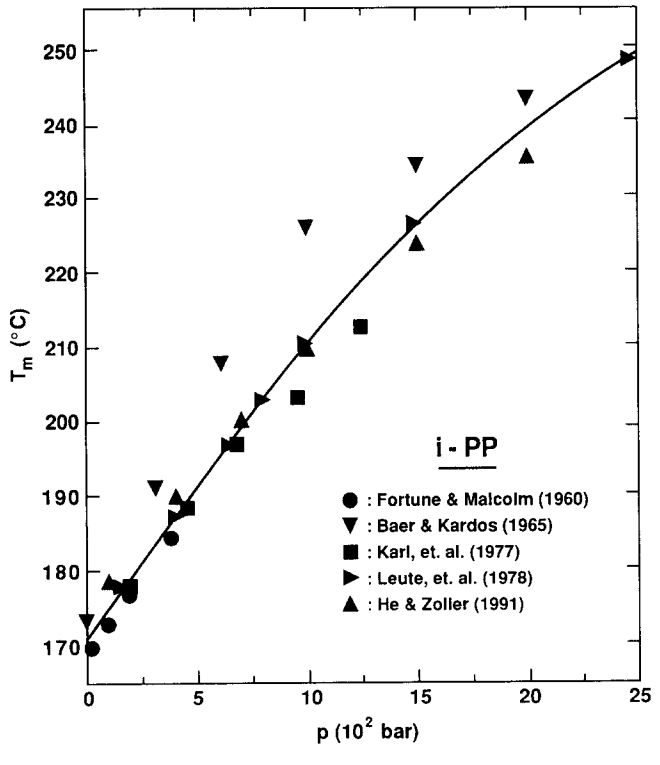

Figure 17 Experimental results for melting temperature of i-PP at elevated pressure based upon data[27,39,69–71] for commercial-grade resins; curve is a graphical fit

Keeping B_1, B_2 and B_3 fixed as given in equation (15), such that curve 0 in *Figure 14* is reproduced at zero gauge pressure, a simplex procedure[68] has been used to iterate upon B_4 and B_5 in order to give the best fit of the elevated-pressure data points shown in *Figure 14*. This has resulted in the following values:

$$B_4 = 4.303 \times 10^{-2}\ \text{C/bar}, \quad B_5 = -9.327 \times 10^{-6}\ \text{C/(bar)}^2 \tag{30}$$

which have been used to generate curves 1–5 in *Figure 14*, corresponding to 100, 500, 1000, 1500 and 2000 bar, respectively.

In considering the constant-cooling-rate data at elevated pressure[27,38,39], it is convenient to plot the results in terms of $T_{1/2}(p)$. This has been done in *Figure 15*. Somewhat surprisingly, it is noted that the results from He and Zoller[27] and Karl *et al.*[39] lie essentially along the same curve even though the respective values of φ differ by more than a factor of two. Based upon *Figure 15*, corresponding results can be constructed for T_{shift} based upon $T_{1/2}(p) - T_{1/2}$ $(p=0)$, as shown plotted as symbols in *Figure 16*. It is noted that the symbols and curve 1 in *Figure 16* are in reasonable agreement, indicating that both the isothermal and constant-cooling-rate crystallization data can be described in terms of the same $T_{shift}(p)$. In turn, it is noted that this result is compatible with the present modelling. That is, if $\lambda(T, p)$ is based upon equations (27) and (28) and is used on the right-hand side of equation (11), then the resulting $\sigma(T, p)$, obtained by integrating equation (11) at fixed elevated pressure, will be characterized by the same shift factor. In turn, based upon equation (16), it follows that the pressure dependence of $T_{1/2}$ (φ, p) will be characterized by the same shift factor.

A further issue concerns whether the empiricism

$$T_{min} \approx (T_m + T_g)/2 \tag{31}$$

still applies at elevated pressure, where $T_{min}(p)$ denotes the temperature at which $\lambda(T, p)$ is a minimum at given p. In terms of equations (27) and (28), it follows that

$$T_{min}(p) = -\frac{B_2}{2B_3} + T_{shift}(p) \tag{32}$$

Concerning $T_m(p)$, corresponding results from the literature[27,39,69–71] are indicated in *Figure 17*. Somewhat surprisingly, the oft-quoted results from Baer and Kardos[70] are seen to be anomalously high relative to the other four sources. In particular, the curve fit in *Figure 17* has been used to construct curve 2 in *Figure 16*, with $T_{shift} = T_m(p) - T_m(0)$ and $T_m(0) \simeq 171$°C. On the other hand, curve 3 in *Figure 16* is based upon data for $T_g(p)$ by Passaglia and Martin[72] obtained for an atactic polypropylene (with 2 or 3% crystallinity) via dilatometry up to pressures of 700 bar. Accordingly, if equation (31) holds at zero gauge pressure, as has been verified in the text for both i-PP and PET, then the question is whether the shift factor for $T_{min}(p)$ is close to the average of the shift factors for $T_m(p)$ and $T_g(p)$. In terms of the results in *Figure 16*, this translates to a comparison between the independent crystallization results, given by curve 1 and symbols, with the average of curves 2 and 3, which is indicated by the dashed curve. It follows that the empiricism seems to be a reasonable approximation at elevated pressures as well.